Inorg. Chem. **2007**, *46*, 6069–6077

Inorganic Chemistry
Article

Solid-State NMR Spectroscopic Study of Coordination Compounds of XeF_2 with Metal Cations and the Crystal Structure of $[Ba(XeF_2)_5][AsF_6]_2$[||]

Michael Gerken,*,[†] Paul Hazendonk,[†] Adriana Iuga,[†] Jared Nieboer,[†] Melita Tramšek,[‡] Evgeny Goreshnik,[‡] Boris Žemva,[‡] Shaohui Zheng,[§] and Jochen Autschbach[§]

Department of Chemistry and Biochemistry, University of Lethbridge, Lethbridge, Alberta T1K 3M4, Canada, Jožef Stefan Institute, Jamova 39, SI-1000 Ljubljana, Slovenia, and University at Buffalo, The State University of New York, Buffalo, New York 14260-3000

Received March 23, 2007

The coordination compounds $[Mg(XeF_2)_2][AsF_6]_2$, $[Mg(XeF_2)_4][AsF_6]_2$, $[Ca(XeF_2)_{2.5}][AsF_6]_2$, $[Ba(XeF_2)_3][AsF_6]_2$, and $[Ba(XeF_2)_5][AsF_6]_2$ were characterized by solid-state ^{19}F and ^{129}Xe magic-angle spinning NMR spectroscopy. The ^{19}F and ^{129}Xe NMR data of $[Mg(XeF_2)_2][AsF_6]_2$, $[Mg(XeF_2)_4][AsF_6]_2$, and $[Ca(XeF_2)_{2.5}][AsF_6]_2$ were correlated with the previously determined crystal structures. The isotropic ^{19}F chemical shifts and $^1J(^{129}Xe–^{19}F)$ coupling constants were used to distinguish the terminal and bridging coordination modes of XeF_2. Chemical-shift and coupling-constant calculations for $[Mg(XeF_2)_4][AsF_6]_2$ confirmed the assignment of terminal and bridging chemical-shift and coupling-constant ranges. The NMR spectroscopic data of $[Ba(XeF_2)_3][AsF_6]_2$ and $[Ba(XeF_2)_5][AsF_6]_2$ indicate the absence of any terminal XeF_2 ligands, which was verified for $[Ba(XeF_2)_5][AsF_6]_2$ by its X-ray crystal structure. The adduct $[Ba(XeF_2)_5][AsF_6]_2$ crystallizes in the space group *Fmmm*, with $a = 11.6604(14)$ Å, $b = 13.658(2)$ Å, $c = 13.7802(17)$ Å, $V = 2194.5(5)$ Å^3 at –73 °C, $Z = 4$, and $R = 0.0350$ and contains two crystallographically independent bridging XeF_2 molecules and one nonligating XeF_2 molecule. The AsF_6^- anions in $[Mg(XeF_2)_4][AsF_6]_2$, $[Ca(XeF_2)_{2.5}][AsF_6]_2$, $[Ba(XeF_2)_3][AsF_6]_2$, and $[Ba(XeF_2)_5][AsF_6]_2$ were shown to be fluxional with the fluorines-on-arsenic being equivalent on the NMR time scale, emulating perfectly octahedral anion symmetry.

Introduction

Soon after the first synthesis of XeF_2, its Lewis basicity was established by the reaction of XeF_2 with strongly Lewis-acidic pentafluorides, such as AsF_5 (eq 1).[1] In the solid state, the crystal structure showed the presence of F−Xe--F--AsF_5 adducts.[2]

$$XeF_2 + AsF_5 \rightarrow [XeF][AsF_6] \quad (1)$$

More recently, xenon difluoride has been found to act as a ligand toward a large variety of Lewis-acidic metal cations, such as alkaline-earth metal cations, e.g., Mg^{2+} [3] and Ca^{2+},[4] the group 14 metal cation, Pb^{2+},[5] transition-metal cations, e.g., Ag^+ [6,7] and Cd^{2+},[8] and lanthanide cations, e.g., Nd^{3+}.[9] Such complexes were prepared as solids from anhydrous HF solution according to eqs 2−4 by either the reactions of the corresponding metal hexafluoropnictates with XeF_2 or upon reaction of the metal fluoride with XeF_2 in the presence of the Lewis acids, BF_3 and PF_5.

$$M(PnF_6)_m + nXeF_2 \rightarrow [M(XeF_2)_n][PnF_6]_m; \quad Pn = P, As, Sb \quad (2)$$

$$MF_m + nXeF_2 + mPF_5 \rightarrow [M(XeF_2)_n][PF_6]_m \quad (3)$$

$$MF_m + nXeF_2 + mBF_3 \rightarrow [M(XeF_2)_n][BF_4]_m \quad (4)$$

* To whom correspondence should be addressed. E-mail: michael.gerken@uleth.ca. Tel: +1-403-329-2173. Fax: +1-403-329-2057.
[†] University of Lethbridge.
[‡] Jožef Stefan Institute.
[§] University at Buffalo.
[||] This paper is dedicated to Professor Neil Bartlett on the occasion of his 75th birthday.

(1) Selig, H.; Holloway, J. H. *Top. Curr. Chem.* **1984**, *124*, 33−90.
(2) Zalkin, A.; Ward, D. L.; Biabioni, R. N.; Templeton, D. H.; Bartlett, N. *Inorg. Chem.* **1978**, *17*, 1318−1322.
(3) Tramšek, M.; Benkič, P.; Žemva, B. *Inorg. Chem.* **2004**, *43*, 699−703.
(4) Benkič, P.; Tramšek, M.; Žemva, B. *Solid State Sci.* **2002**, *4*, 1425−1434.
(5) Tramšek, M.; Benkič, P.; Žemva, B. *Solid State Sci.* **2002**, *4*, 9−14.
(6) Hagiwara, R.; Hollander, F.; Maines, C.; Bartlett, N. *Eur. J. Solid State Inorg. Chem.* **1991**, *28*, 855−866.

10.1021/ic700557m CCC: $37.00 © 2007 American Chemical Society

Published on Web 06/22/2007

Table 1. Solid-State NMR Spectroscopic Data for $[Mg(XeF_2)_2][AsF_6]_2$, $[Ca(XeF_2)_{2.5}][AsF_6]_2$, $[Ba(XeF_2)_3][AsF_6]_2$, and $[Ba(XeF_2)_5][AsF_6]_2$

^{19}F				^{129}Xe	
δ_{iso}, ppm	$\Delta\sigma$, ppm (η)	$^1J(^{129}Xe-^{19}F)$, Hz	assignment	δ_{iso}, ppm	$\Delta\sigma$, ppm (η)
		$[Mg(XeF_2)_2][AsF_6]_2$			
−240.4	102 ± 3 (0)	−6200	$F_{terminal}$	−1219 ± 2	4760 ± 25 (0)
−206.5	102 ± 3 (0)	−5550	$F_{bridging}$		
		$[Ca(XeF_2)_{2.5}][AsF_6]_2$			
−205.6	101 (0)	−5890	$F_{bridging}$	−1123	4860 (0)
−203.1	101 (0)	−5670	$F_{bridging}$		
−201.6	101 (0)	−5710	$F_{bridging}$		
−187.0	101 (0)	−5550	$F_{bridging}$		
−177.5	101 (0)	−5600	$F_{bridging}$		
		$[Ba(XeF_2)_3][AsF_6]_2$			
−193.0	134 ± 2 (0.5)	−5550 ± 50	$F_{bridging}$	−1340 ± 2	4660 ± 80 (0.1)
−189.9	137 ± 2 (0.5)	−5680 ± 50	$F_{bridging}$	−1310 ± 2	4660 ± 80 (0.1)
−186.1	147 ± 2 (0.5)	−5800 ± 50	$F_{bridging}$	−1275 ± 2	4330 ± 80 (0.1)
−183.0	157 ± 2 (0.5)	−5740 ± 50	$F_{bridging}$		
		$[Ba(XeF_2)_5][AsF_6]_2$			
−184.4	121 (0.5)	−5790	$F_{bridging}$	−1470	4490 (0.1)
−174.8	115 (0.5)	−5700	$F_{bridging}$	−1314	4440 (0)
−173.9	121 (0.5)	−5650	$F_{bridging}$		

The coordination environment about the metal cations in such complexes is comprised of fluorine atoms from (a) XeF_2 ligands and the PnF_6^- (Pn = As, Sb, P) or BF_4^- counter-anions or (b) exclusively XeF_2 ligands.[10] Xenon difluoride exhibits two coordination modes; i.e., it can act as a terminal ligand, found in $[Mg(XeF_2)_n][AsF_6]_2$ ($n = 2, 4$),[3] where only one fluorine of an XeF_2 molecule coordinates to the metal cation, and as a bridging ligand, found in $[Ca(XeF_2)_{2.5}][AsF_6]_2$,[4] where both fluorine atoms of an XeF_2 molecule coordinate to separate metal cations. Even though Raman spectroscopy has been used to predict the nature of XeF_2 ligands, X-ray crystallography remains the only means to unambiguously determine the coordination mode of XeF_2 in these complexes.

Although solution-state ^{19}F and ^{129}Xe NMR spectroscopy has been instrumental in characterizing many xenon fluorides,[11] it cannot provide structural information about coordination compounds of XeF_2 with metal cations, since in solution these adducts either dissociate or are fluxional on the NMR time scale. Due to the recent progress in the solid-state NMR spectroscopic characterization of xenon fluorides,[12,13] ^{19}F and ^{129}Xe magic-angle spinning (MAS) NMR spectroscopy was utilized as a spectroscopic tool to elucidate the structures of coordination compounds where crystal growth has been unsuccessful, using an encapsulation methodology for the moisture-sensitive samples.[12]

(7) Matsumoto, K.; Hagiwara, R.; Ito, Y.; Tamada, O. *Solid State Sci.* **2002**, *4*, 1465−1469.
(8) Tavčar, G.; Benkič, P.; Žemva, B. *Inorg. Chem.* **2004**, *43*, 1452−1457.
(9) Tramšek, M.; Lork, E.; Mews, R.; Žemva, B. *J. Solid State Chem.* **2001**, *162*, 243−249.
(10) Tramšek, M.; Benkič, P.; Žemva, B. *Angew. Chem.* **2004**, *116*, 3538−3540. Tramšek, M.; Benkič, P.; Žemva, B. *Angew. Chem., Int. Ed.* **2004**, *43*, 3456−3458.
(11) Gerken, M.; Schrobilgen, G. J. *Coord. Chem. Rev.* **2000**, *197*, 335−395.
(12) Gerken, M.; Hazendonk, P.; Nieboer, J.; Schrobilgen, G. J. *J. Fluorine Chem.* **2004**, *125*, 1163−1168.
(13) Forgeron, M. A. M.; Wasylishen, R. E.; Penner, G. H. *J. Phys. Chem. A* **2004**, *108*, 4751−4758.

Results and Discussion

To establish trends in NMR parameters, three coordination compounds with known structures were investigated by ^{19}F and ^{129}Xe NMR spectroscopy: $[Mg(XeF_2)_2][AsF_6]_2$,[3] $[Mg(XeF_2)_4][AsF_6]_2$,[3] and $[Ca(XeF_2)_{2.5}][AsF_6]_2$,[4] which contain exclusively terminal (Mg^{2+} salts) or exclusively bridging XeF_2 ligands (Ca^{2+} salt). In addition, two coordination compounds of previously unknown structures, $[Ba(XeF_2)_3][AsF_6]_2$ and $[Ba(XeF_2)_5][AsF_6]_2$, were characterized to predict the coordination modes of XeF_2 based on NMR spectroscopic parameters. The nature of the samples prepared for this NMR study was verified by X-ray powder diffraction (Mg^{2+} salts) and Raman spectroscopy (Mg^{2+}, Ca^{2+}, and Ba^{2+} salts). On the basis of a number of well-resolved NMR resonances and their lineshapes, the presence of different crystallographic modifications was excluded for these samples. The isotropic chemical shifts, $\delta_{iso}(^{19}F)$ and $\delta_{iso}(^{129}Xe)$, the shielding tensor parameters (anisotropies, $\Delta\sigma$, and asymmetries, η), and the $^1J(^{129}Xe-^{19}F)$ coupling constants obtained from the ^{19}F NMR spectra are listed in Table 1. The ^{19}F and ^{129}Xe NMR parameters for $[Mg(XeF_2)_4][AsF_6]_2$ are listed separately in Tables 2 and 3, respectively, together with the calculated values. The present study uses the following conventions for the isotropic shielding (eq 5), the shielding anisotropy (eq 6), and the asymmetry (eq 7):[14]

$$\sigma_{iso} = {}^1/_3(\sigma_{33} + \sigma_{22} + \sigma_{11}) \quad (5)$$

$$\Delta\sigma = \sigma_{33} - {}^1/_2(\sigma_{22} + \sigma_{11}) \quad (6)$$

$$\eta = (\sigma_{22} - \sigma_{11})/(\sigma_{33} - \sigma_{iso}) \quad (7)$$

The isotropic chemical shifts, $\delta_{iso}(^{19}F)$, and coupling constants, $^1J(^{75}As-^{19}F)$, for the anionic ^{19}F environments are listed in Table 4.

Fluorine-19 MAS NMR Spectroscopy. $[Mg(XeF_2)_2][AsF_6]_2$. The crystal structure of $[Mg(XeF_2)_2][AsF_6]_2$ shows

(14) Spiess, H. W. In *NMR Basic Principles and Progress*; Diehl, P., Fluck, E., Kosfeld, R., Eds.; Springer-Verlag: Berlin, 1978; Vol. 15, p 76.

Table 2. Experimental and Calculated Values for $\delta_{iso}(^{19}F)$, $\Delta\sigma$, η, and $^{1}J(^{129}Xe-^{19}F)$ of $[Mg(XeF_2)_4][AsF_6]_2$ Together with the Assignment to the Crystallographic Fluorine Sites

experimental			calculated[a]			$^{1}J(^{129}Xe-^{19}F)$ Hz		assignment[c]	
$\delta_{iso}(^{19}F)$ (ppm)	$\Delta\sigma$ (ppm)	η	$\delta_{iso}(^{19}F)$ (ppm)	$\Delta\sigma$ (ppm)	η	experimental	calculated[b]		
−206.6	115	0.2	−200	152	0.18	−5150	−4636	F1	bridging
−218.5	124	0.1	−201	163	0.12	−6000	−4734	F2	bridging
−206.6	115	0.2	−189	158	0.20	−5150	−4533	F3	bridging
−197.7	121	0.1	−187	164	0.10	−5600	−4514	F4	bridging
−234.1	96	0.3	−246	136	0.06	−6230	−5579	F5	terminal
−221.9	127	0.1	−221	166	0.09	−6000	−5781	F6	terminal
−226.5	124	0.2	−242	137	0.04	−6000	−5627	F7	terminal
−233.5	105	0.2	−243	136	0.06	−6250	−5683	F8	terminal

[a] Calculated at BP86/TZ2P/ZSO level of theory based on experimental structure. With a geometry optimized at the BP86/TZ2P/ZSC level, we obtained the following chemical shifts in ppm: F1 = −168, F2 = −162, F3= −167, F4 = −172, F5 = −199, F6 = −193, F7 = −193, and F8= −197. [b] Calculated at BP86/TZ2P/ZSC level based on experimental structure. With a geometry optimized at the BP86/TZ2P/ZSC level, we obtained the following spin−spin coupling constants in Hz: ^{1}J(Xe−F1) = −4513, ^{1}J(Xe−F2) = −4559, ^{1}J(Xe−F3) = −4531, ^{1}J(Xe−F4) = −4658, ^{1}J(Xe−F5) = −6137, ^{1}J(Xe−F6) = −5988, ^{1}J(Xe−F7) = −6046, and ^{1}J(Xe−F8) = −6016. [c] Atom numbering from ref 3.

Table 3. Experimental and Calculated Values for $\delta(^{129}Xe)$, $\Delta\sigma$, and η of $[Mg(XeF_2)_4][AsF_6]_2$ Together with the Assignment to the Crystallographic Xenon Sites

experimental			calculated[a]			
$\delta_{iso}(^{129}Xe)$ (ppm)	$\Delta\sigma$ (ppm)	η	$\delta_{iso}(^{129}Xe)$ (ppm)	$\Delta\sigma$ (ppm)	η	assignment[b]
−1157	4730	0	−1736	6194	0.02	Xe1
−1120	4540	0	−1656	6377	0.02	Xe2
−1157	4730	0	−1720	6206	0.02	Xe3
−1157	4730	0	−1710	6254	0.015	Xe4

[a] Calculated at the BP86/TZ2P/ZSO level of theory based on experimental geometry. [b] Atom numbering from ref 3.

Table 4. Fluorine-19 Solid-State NMR Spectroscopic Data of Fluorine-on-Arsenic for $[Mg(XeF_2)_4][AsF_6]_2$, $[Ca(XeF_2)_{2.5}][AsF_6]_2$, $[Ba(XeF_2)_3][AsF_6]_2$, and $[Ba(XeF_2)_5][AsF_6]_2$

compound	$\delta_{iso}(^{19}F)$ (ppm)	$^{1}J(^{75}As-^{19}F)$ (Hz)	ratio of integral	assignment with respect to crystal structures[a]
$[Mg(XeF_2)_4][AsF_6]_2$	−63.4	920	1	$As1F_6^-$, $As2F_6^-$
	−64.5	920	1	
$[Ca(XeF_2)_{2.5}][AsF_6]_2$	−58.0	930	2	$As2F_6^-$
	−60.7	930	1	$As1F_6^-$
$[Ba(XeF_2)_3][AsF_6]_2$	−55.6	946	1	[b]
	−58.5	946	1	[b]
	−59.5	946	1	[b]
	−60.0	946	2	[b]
	−60.2	946	2	[b]
	−61.5	946	1	[b]
$[Ba(XeF_2)_5][AsF_6]_2$	−58.6	950		$As1F_6^-$

[a] Atom numbering from refs 3, 4, and present study. [b] No crystal structure available.

Mg^{2+} coordinated by XeF_2 and AsF_6^- anions.[3] The coordination environment about Mg^{2+} is pseudo-octahedral with two fluorines from terminal XeF_2 ligands and four fluorine atoms from four AsF_6^- anions. Because of crystallographic symmetry (orthorhombic space group *Pbam*), both XeF_2 ligands are equivalent and result in one crystallographically unique coordinating fluorine and one terminal fluorine environment. All AsF_6^- anions in the unit cell are also crystallographically identical. The ^{19}F MAS NMR spectrum of $[Mg(XeF_2)_2][AsF_6]_2$ shows spinning-sideband manifolds for two fluorine environments with xenon satellites (Figure 1) and a very broad unresolved signal in the fluorine-on-arsenic chemical-shift region at ca. −65 ppm (Figure 2), indicating motion of the AsF_6^- anion on the NMR time scale or broadening of the ^{19}F resonances by interactions with the large quadrupolar

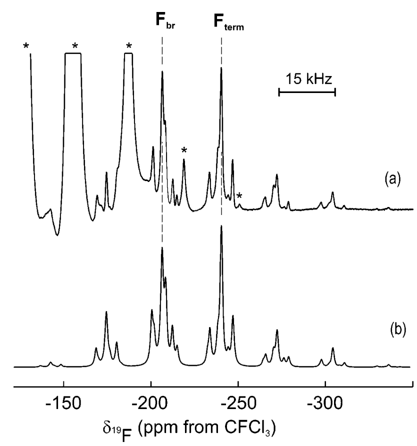

Figure 1. (a) Experimental and (b) simulated solid-state ^{19}F MAS NMR spectrum of $[Mg(XeF_2)_2][AsF_6]_2$, recorded at a spinning rate of 15 kHz at −10 °C. Asterisks (*) denote the spinning-sideband manifold of FEP.

coupling constant on ^{75}As (100%, $I = ^{3}/_{2}$). An early ^{19}F MAS NMR spectrum of polycrystalline $KAsF_6$ showed a 1:1:1:1 quartet with a $^{1}J(^{75}As-^{19}F)$ coupling constant of 905 Hz.[15] The resolved equal-intensity quartet reflects the octahedral shape of the AsF_6^- anion in $KAsF_6$. The two ^{19}F-on-Xe resonances have distinctly different isotropic chemical shifts (−240 and −206 ppm) and $^{1}J(^{129}Xe-^{19}F)$ coupling constants (−6200 and −5550 Hz), which can be assigned to the terminal and bridging fluorine environments, respectively. Upon terminal coordination of XeF_2, the XeF_2 ligand is polarized, resulting in a stronger terminal Xe−F bond and a weaker bridging Xe--F bond (Chart 1).

Chart 1

$$Mg^{2+}\cdots F_{br}\text{--}Xe-F_{term}$$

As a direct consequence, the absolute value of the $^{1}J(^{129}Xe-^{19}F)$ coupling constant of the $Xe-F_{term}$ bond increases and $\delta_{iso}(^{19}F_{term})$ shifts to lower frequency, compared with XeF_2 (solid state: $\delta_{iso}(^{19}F) = -169$ ppm; $^{1}J(^{129}Xe-^{19}F) = -5550$ Hz).[12] The isotropic shift and the ^{1}J coupling constant of the $Xe-F_{term}$ moiety move toward the values

(15) Andrew, E. R.; Farnell, L. F.; Gledhill, T. D. *Phys. Rev. Lett.* **1967**, *19*, 6−7.

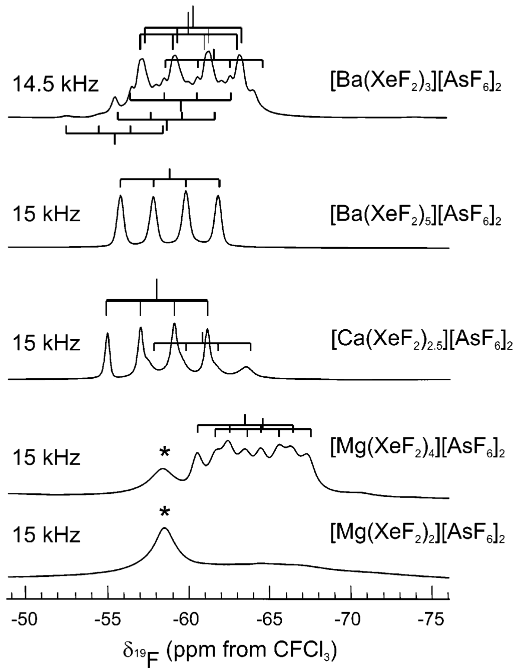

Figure 2. Fluorine-on-arsenic region of the solid-state ^{19}F MAS NMR spectrum of $[Mg(XeF_2)_2][AsF_6]_2$, $[Mg(XeF_2)_4][AsF_6]_2$, $[Ca(XeF_2)_{2.5}][AsF_6]_2$, $[Ba(XeF_2)_3][AsF_6]_2$, and $[Ba(XeF_2)_5][AsF_6]_2$, recorded at specified spinning rates and at −10 °C. Asterisks (*) denote the spinning-sideband manifold of FEP.

found for the XeF^+ cation in solution ($\delta(^{19}F) = -242.5$ to -294.5 ppm; $^1J(^{129}Xe-^{19}F) = -6615$ to -7594 Hz) compared with uncoordinated XeF_2.[11] The NMR data for both fluorine environments in the adduct lie between those for XeF_2(s) and XeF^+(solv), with δ_{iso} and $^1J(^{129}Xe-^{19}F)$ for the bridging fluorine being closer to the values found for XeF_2.

The intensities of the ^{129}Xe satellites in both spinning-sideband manifolds are asymmetric, as a consequence of cross terms between the $^{129}Xe-^{19}F$ dipolar coupling, R_{DD}, and the scalar, indirect coupling, J. The direction of the slanting of the satellites is determined by the relative signs of R_{DD} and J. This slanting in the ^{19}F NMR spectrum of $[Mg(XeF_2)_2][AsF_6]_2$ can only be reproduced for opposite signs of R_{DD} and J. As R_{DD} (eq 8) is positive, $^1J(^{129}Xe-^{19}F)$ must have a negative sign, which confirms the prediction of

$$R_{DD} = \frac{\mu_0 \hbar}{4\pi 2\pi} \gamma_A \gamma_B \langle r_{AB}^{-3} \rangle \quad (8)$$

negative $^1J(^{129}Xe(II)-^{19}F)$ coupling constants based on an empirical correlation,[11] which has subsequently been supported by theoretical calculations.[16] An average R_{DD} value of 4800 Hz was calculated from the average Xe−F bond distances and was used in all spectral simulations, giving good agreement between simulated and experimental spectra. The experimental spectra actually contain information about the effective dipolar coupling constant, R_{eff}, which is related to R_{DD} via the anisotropy in J, ΔJ (eq 9). The experimental intensities of the satellites, however, did not allow for the accurate determination of R_{eff}, which is significantly different

$$R_{eff} = R_{DD} - \frac{\Delta J}{3} \quad (9)$$

from average R_{DD}. As a consequence, ΔJ was neglected in the present study. In a previous study of solid XeF_2, a ΔJ value of 2370 Hz was determined.[13] The shielding anisotropies for both fluorine environments do not exhibit significant differences. This is surprising, as it is expected that the polarization of the bridging fluorine atom by the metal cation would render its shielding tensor significantly different from that of the terminal fluorine. Distortions of the spinning-sideband patterns due to the presence of the fluoropolymer background signal introduce significant uncertainty in the analysis, making subtle differences in shielding tensors difficult to discern.

$[Mg(XeF_2)_4][AsF_6]_2$. As in $[Mg(XeF_2)_2][AsF_6]_2$, X-ray crystallography showed that $[Mg(XeF_2)_4][AsF_6]_2$ contains exclusively terminal XeF_2 ligands (Chart 1).[3] The Mg^{2+} cation in $[Mg(XeF_2)_4][AsF_6]_2$ is surrounded by four fluorine atoms from crystallographically different XeF_2 ligands and two fluorine atoms from two crystallographically different AsF_6^- anions. The crystal structure contains, in total, eight crystallographically different F-on-Xe environments: four coordinating/bridging and four terminal fluorines. The ^{19}F MAS NMR spectrum of $[Mg(XeF_2)_4][AsF_6]_2$ is complicated, containing seven isotropic signals with ^{129}Xe satellites, a singlet at −195 ppm for unreacted MgF_2 (ca. 60 mol % based on Mg^{2+}), a singlet at −188 ppm for an unidentified impurity (2.4 times the intensity of one fluorine-on-xenon site) (Figure 3), and two overlapping 1:1:1:1 quartets in the F-on-As region (Figure 2). In solution, where the molecular environments are highly fluxional due to rapid tumbling and diffusion of solute and solvent molecules, molecules of the same type experience the same time-averaged solvent environment and give rise to one resonance for each chemically unique nucleus. In the solid state, on the other hand, molecules are locked into positions of a particular crystallographic environment and each crystallographically unique species in the unit cell will give rise to a separate NMR resonance. The ^{19}F MAS NMR spectrum of $[Mg(XeF_2)_4][AsF_6]_2$ is in excellent agreement with the crystal structure. The eight unique F-on-Xe atoms in the unit cell of $[Mg(XeF_2)_4][AsF_6]_2$ can be correlated to the seven isotropic ^{19}F signals with ^{129}Xe satellites, where the signal at −206 ppm corresponds to two fluorine sites. The isotropic chemical shifts of the ^{19}F resonances with ^{129}Xe satellites span frequency ranges attributable to terminal fluorines and bridging fluorines. The almost continuous range of isotropic ^{19}F-on-Xe chemical shifts indicate variable strengths of coordination, with especially one XeF_2 being weakly polarized. Density-functional theory (DFT) calculations of the chemical shifts and spin−spin coupling constants confirm the general assignment of bridging and terminal fluorine environments and allow for a tentative assignment of crystallographic fluorine environments to ^{19}F resonances (see Calculations).

The two resonances centered at −63.4 and −64.5 ppm are split into 1:1:1:1 quartets caused by $^1J(^{75}As-^{19}F)$ coupling

(16) Bryce, D. L.; Wasylishen, R. E. *Inorg. Chem.* **2002**, *41*, 3091−3101.

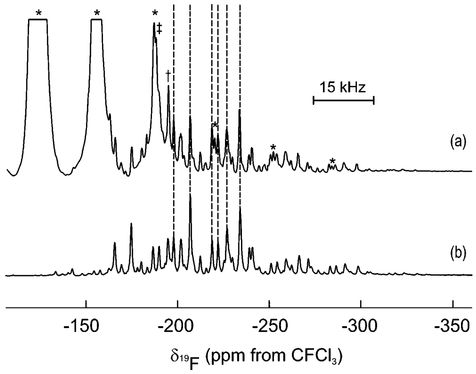

Figure 3. (a) Experimental and (b) simulated solid-state ^{19}F MAS NMR spectrum of $[Mg(XeF_2)_4][AsF_6]_2$, recorded at a spinning rate of 15 kHz at −10 °C. Asterisks (*) denote the spinning-sideband manifold of FEP. Dagger (†) and double dagger (‡) denote the signals associated with MgF_2 and an unidentified impurity, respectively.

(920 Hz) and can be attributed to the two crystallographically different AsF_6^- anions. The chemical shift and indirect spin−spin coupling constant compare very well with those found in solution ($\delta(^{19}F) = -64.3$ ppm; $^1J(^{75}As-^{19}F) = 932$ Hz).[17] The $^1J(^{75}As-^{19}F)$ coupling constant is also in good agreement with that found for solid $KAsF_6$ (905 Hz).[15] In cases where ^{19}F is bonded to a quadrupolar nucleus, second-order quadrupolar effects can be observed in the ^{19}F NMR spectrum if the quadrupolar coupling constant, $\chi = e^2Qq_{33}/h$, with Q being the quadrupole moment and q_{33} being the largest component of the electric field gradient, is sufficiently large. In such cases, fast MAS does not remove heteronuclear dipolar coupling between ^{19}F and the quadrupolar nucleus. For mild interactions, the equal-intensity multiplet shows asymmetry, with spacings on one side being smaller and larger on the other side compared with the J constant. Such asymmetric multiplets have been observed for K_2NbF_7[18] and $Cdpy_4NbOF_5$.[19] If χ is very large, the quadrupole interaction cannot be considered as a perturbation of the Zeeman term anymore, since it becomes of the same or of larger size. As a consequence, severe distortions of the ^{19}F resonances arise, as observed recently for the $IO_2F_2^-$ anion.[20] Surprisingly, no asymmetry was observed for the quartets of the AsF_6^- anion in $[Mg(XeF_2)_4][AsF_6]_2$, indicating a negligible χ, because of a small electrical field gradient on arsenic, arising from an octahedral arsenic environment. The perfectly octahedral geometry and the equivalence of all six fluorines on each AsF_6^- anion on the NMR time scale are in contrast to the crystallographic finding, indicating rapid reorientation of the AsF_6^- anion in the crystal structure, emulating a perfectly octahedral anion.

$[Ca(XeF_2)_{2.5}][AsF_6]_2$. The crystal structure of $[Ca(XeF_2)_{2.5}]$-$[AsF_6]_2$ contains three crystallographically different bridging XeF_2 ligands with five crystallographically different bridging fluorines bonded to xenon (Chart 2).[4] The coordination

Chart 2

$$Ca^{2+}\cdots F\text{--}Xe\text{--}F\cdots Ca^{2+}$$

number of Ca^{2+} is nine, with six fluorines from XeF_2 ligands and three fluorines from AsF_6^- anions coordinating toward Ca^{2+}. Five fluorines bonded to xenon and one-and-one-half AsF_6^- anions are present in the asymmetric unit. In agreement with the crystal structure, the ^{19}F NMR spectrum shows five resonances with ^{129}Xe satellites (Figure S1 in the Supporting Information). The chemical-shift range (−206 to −178 ppm) and the range of $^1J(^{129}Xe-^{19}F)$ coupling constants (−5550 to −5890 Hz) are in agreement with the bridging nature of the XeF_2 ligands and the absence of any terminal Xe−F moiety. Two overlapping 1:1:1:1 quartets are observed at −58.0 and −60.7 ppm in a 2:1 ratio (Figure 2). These two quartets can be correlated to the $As(2)F_6^-$ and to $As(1)F_6^-$ anions found in a 2:1 ratio in the unit cell, respectively. Both fluorine-on-arsenic resonances exhibit $^1J(^{75}As-^{19}F)$ couplings of 930 Hz. No asymmetry was observed, indicating rapid reorientation of the AsF_6^- anions in the solid state, as found for $[Mg(XeF_2)_4][AsF_6]_2$.

$[Ba(XeF_2)_3][AsF_6]_2$. To date, no crystals suitable for X-ray crystallography could be grown for $[Ba(XeF_2)_3][AsF_6]_2$. Four separate ^{19}F resonances with ^{129}Xe satellites were observed in the ^{19}F MAS NMR spectrum of $[Ba(XeF_2)_3][AsF_6]_2$ in the range of −193 to −183 ppm (Figure S2 in the Supporting Information), indicating the presence of four crystallographically different fluorine-on-xenon environments. The chemical-shift range suggests the absence of terminal Xe−F moieties. This is supported by the $^1J(^{129}Xe-^{19}F)$ coupling constants (−5550 to −5740 Hz). The fluorine-on-arsenic chemical-shift region shows six overlapping 1:1:1:1 quartets in a 1(−55.6 ppm):1(−58.5 ppm):1(−59.5 ppm):2(−60.0 ppm):2(−60.2 ppm):1(−61.5 ppm) ratio (Figure 2). The $^1J(^{75}As-^{19}F)$ coupling constants for all six quartets are 946 Hz, with no asymmetry observed. On the basis of solid-state NMR spectroscopic information, the asymmetric unit of $[Ba(XeF_2)_3][AsF_6]_2$ should contain four fluorines bonded to xenon, two complete AsF_6^- anions, and four halves of AsF_6^- anions, which have to be located on special positions.

$[Ba(XeF_2)_5][AsF_6]_2$. The ^{19}F MAS NMR spectrum of $[Ba(XeF_2)_5][AsF_6]_2$ shows three signals in the fluorine-on-xenon chemical-shift range (−184 to −174 ppm) with ^{129}Xe satellites ($^1J(^{129}Xe-^{19}F) = -5650$ to -5790 Hz) (Figure S3 in the Supporting Information), suggesting the absence of terminal fluorine-on-xenon environments. The fluorine-on-arsenic region comprises one 1:1:1:1 quartet at −58.6 ppm ($^1J(^{75}As-^{19}F) = 950$ Hz), corresponding to one crystallographically unique AsF_6^- anion, which rearranges fast on the NMR time scale (Figure 2). These predictions are in accordance with the X-ray crystal structure of $[Ba(XeF_2)_5]$-$[AsF_6]_2$ (see X-ray Crystal Stucture of $[Ba(XeF_2)_5][AsF_6]_2$), which was obtained for this study, showing the presence of two bridging fluorines-on-xenon and one fluorine-on-xenon in uncoordinated XeF_2 in the asymmetric unit. The ^{19}F chemical shift of fluorine on nonligating XeF_2 and bridging fluorine-on-xenon environments have similar chemical shifts

(17) Dove, M. F. A.; Sanders, J. C. P.; Jones, E. L.; Parkin, M. J. *J. Chem. Soc., Chem. Commun.* **1984**, 1578−1581.
(18) Du, L.-S.; Schurko, R. W.; Lim, K. H.; Grey, C. P. *J. Phys. Chem. A* **2001**, *105*, 760−768.
(19) Du, L.-S.; Schurko, R. W.; Kim, N.; Grey, C. P. *J. Phys. Chem. A* **2002**, *106*, 7876−7886.
(20) Gerken, M.; Hazendonk, P.; Iuga, A.; Mack, J. P.; Mercier, H. P. A.; Schrobilgen, G. J. *J. Fluorine Chem.* **2006**, *127*, 1328−1338.

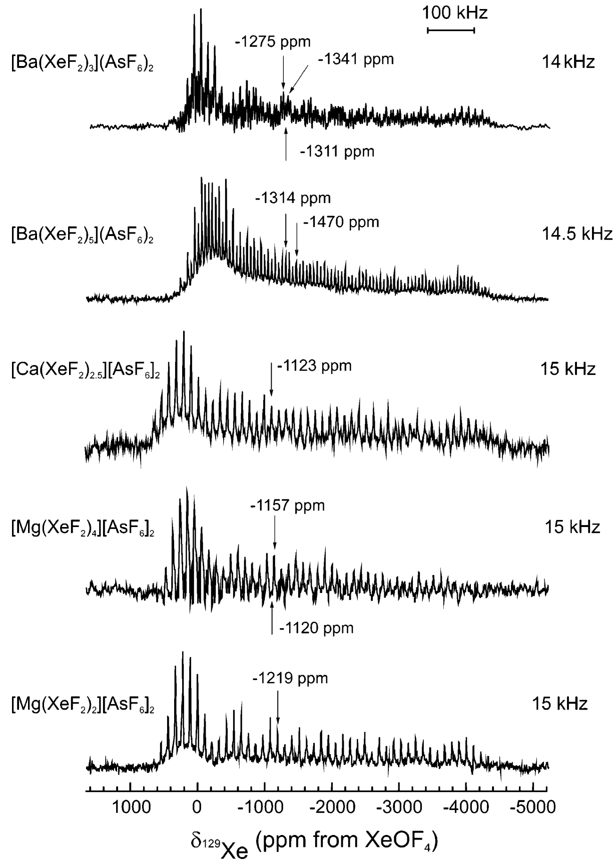

Figure 4. Solid-state ^{129}Xe MAS NMR spectrum of $[Mg(XeF_2)_2][AsF_6]_2$, $[Mg(XeF_2)_4][AsF_6]_2$, $[Ca(XeF_2)_{2.5}][AsF_6]_2$, $[Ba(XeF_2)_3][AsF_6]_2$, and $[Ba(XeF_2)_5][AsF_6]_2$, recorded at specified spinning rates and at −10 °C.

and cannot be distinguished solely based on chemical shift and *J* coupling constant information.

Xenon-129 MAS NMR Spectroscopy. The ^{129}Xe{^{19}F} NMR spectra of all five coordination compounds of XeF_2 that were studied in this paper are depicted in Figure 4 and give rise to spinning-sideband manifolds with shielding anisotropies significantly larger than that observed for neat XeF_2(s) (4260 ppm), ranging from 4330 to 4860 ppm.[12] The linear geometry about xenon results in nearly axial-symmetric shielding tensors for xenon in all coordination compounds in this study. The ^{129}Xe chemical shifts of coordinated XeF_2 are shifted to higher frequencies compared with $\delta(^{129}Xe)$ of neat XeF_2(s). No obvious correlation between coordination mode and chemical shift could be established, presumably because of the extreme sensitivity of ^{129}Xe to changes in the environment due to packing and nonbonded interactions, in addition to the coordination mode of the XeF_2 ligand.

While the line-width of the ^{129}Xe lines ($\Delta\nu_{1/2} = 2800$ Hz) did not allow the observation of different isotropic chemical shifts for the five crystallographically different xenon atoms in $[Ca(XeF_2)_{2.5}][AsF_6]_2$, two sets of spinning-sideband manifolds were observed for $[Mg(XeF_2)_4][AsF_6]_2$ in a 3:1 ratio, correlating to the four different xenon atoms found in the crystal structure, which is in accord with the ^{129}Xe chemical shift calculations (see Calculations). The ^{129}Xe NMR data for $[Mg(XeF_2)_4][AsF_6]_2$ suggest the presence of one distinctly different XeF_2 ligand in the structure. In the ^{129}Xe NMR spectrum of $[Ba(XeF_2)_3][AsF_6]_2$, three different xenon environments could be resolved with isotropic chemical shifts of −1340, −1310, and −1275 ppm. This indicates at least three crystallographically unique xenon atoms in the unit cell, which is consistent with the prediction of a larger asymmetric unit that contains four fluorine-on-xenon atoms and six arsenic atoms. This large unit cell can serve as an explanation for the difficulty of growing crystals of $[Ba(XeF_2)_3][AsF_6]_2$.

Table 5. Summary of Crystal Data and Refinement Results for $[Ba(XeF_2)_5][AsF_6]_2$

formula	$As_2Ba\,F_{22}Xe_5$
T (°C)	−73
space group	*Fmmm* (no. 69)
a (Å)	11.6604(14)
b (Å)	13.658(2)
c (Å)	13.7802(17)
V (Å^3)	2194.5(5)
Z (molecules/unit cell)	4
calcd density (g/cm^3)	4.119
λ (Å)	0.71069
μ (mm^{-1})	12.555
R_1,^{a} R_2^{b}	0.035, 0.1011

^{a} $R_1 = \Sigma|F_o| - |F_c|/\Sigma|F_o|$. ^{b} $R_2 = \Sigma(|F_o| - |F_c|)w^{1/2}/\Sigma|F_o|w$.

Table 6. Selected Bond Lengths in $[Ba(XeF_2)_5][AsF_6]_2$

bond	distance (Å)^a
Ba1−F2^{i}, Ba1−F2^{ii}, Ba1−F2, Ba1−F2^{iii}	2.700(5)
Ba1−F11^{iii}, Ba1−F11, Ba1−F11^{i}, Ba1−F11^{ii}	2.868(4)
Ba1−F3^{iv}, Ba1−F3^{v}, Ba1−F3^{iii}, Ba−F3	2.973(6)
Xe1−F1^{vi}, Xe1−F1^{vii}	1.994(8)
Xe2−F2, Xe2−F2^{viii}	2.005(5)
Xe3−F3, Xe3−F3^{ix}	1.995(5)
As1−F12, As1−F12^{x}, As1−F12^{v}, As1−F12^{xi}	1.686(4)
As1−F11, As1−F11^{x}	1.724(4)

^{a} Symmetry codes: (i) $1 - x, y, z$; (ii) $x, 1 - y, 1 - z$; (iii) $1 - x, 1 - y, 1 - z$; (iv) $1 - x, y, 1 - z$; (v) $x, 1 - y, z$; (vi) $^3/_2 - x, 1 - y, ^1/_2 - z$; (vii) $^1/_2 + x, y, ^1/_2 + z$; (viii) $^3/_2 - x, ^1/_2 - y, 1 - z$; (ix) $1 - x, ^3/_2 - y, ^1/_2 - z$; (x) $^3/_2 - x, 1 - y, ^3/_2 - z$; (xi) $^3/_2 - x, y, ^3/_2 - z$; (xii) $x - ^1/_2, y, z - ^1/_2$.

X-ray Crystal Structure of $[Ba(XeF_2)_5][AsF_6]_2$. The $[Ba(XeF_2)_5][AsF_6]_2$ salt was found to be isostructural with $[Ba(XeF_2)_5][SbF_6]_2$, both crystallizing in the orthorhombic space group *Fmmm*. Crystallographic details and selected bond distances for $[Ba(XeF_2)_5][AsF_6]_2$ are given in Tables 5 and 6. The unit cell of $[Ba(XeF_2)_5][AsF_6]_2$ contains three crystallographically unique XeF_2 molecules; two of these molecules act as ligands bridging two Ba^{2+} centers, while one XeF_2 molecule is incorporated in the crystal lattice without any contacts to Ba^{2+}. In addition, one crystallographically unique AsF_6^- anion is found in the unit cell, confirming the findings of solid-state NMR spectroscopy (see Fluorine-19 MAS NMR Spectroscopy). As in $[Ba(XeF_2)_5][SbF_6]_2$,[21] barium in $[Ba(XeF_2)_5][AsF_6]_2$ has a coordination number of 12, being surrounded by three sets of four symmetry-related fluorine atoms: F2, F3 (both from XeF_2 molecules), and F11

(21) The structure of $[Ba(XeF_2)_5][SbF_6]_2$, described in the monoclinic *C*2/*m* space group, was published in 2002. After the structure of $[Ba(XeF_2)_5][AsF_6]_2$ was solved, the high similarity of both structures sparked the reinvestigation of the structure of $[Ba(XeF_2)_5][SbF_6]_2$, and it was found that the space group of $[Ba(XeF_2)_5][SbF_6]_2$ had previously been misassigned. The correct space group of $[Ba(XeF_2)_5][SbF_6]_2$ is *Fmmm*, with the AsF_6^- and SbF_6^- salts being isostructural. The corrected crystallographic details (CIF file and selected bond distances) for $[Ba(XeF_2)_5][SbF_6]_2$ are given in the Supporting Information. Turičnik, A.; Benkič, P.; Žemva, B. *Inorg. Chem.* **2002**, *41*, 5521−5524.

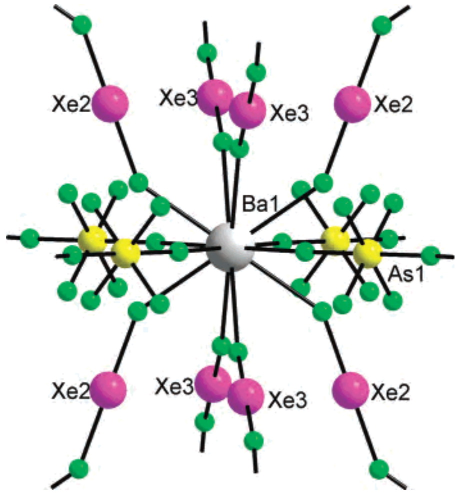

Figure 5. Coordination sphere of the barium atom in the structure of $[Ba(XeF_2)_5][AsF_6]_2$.

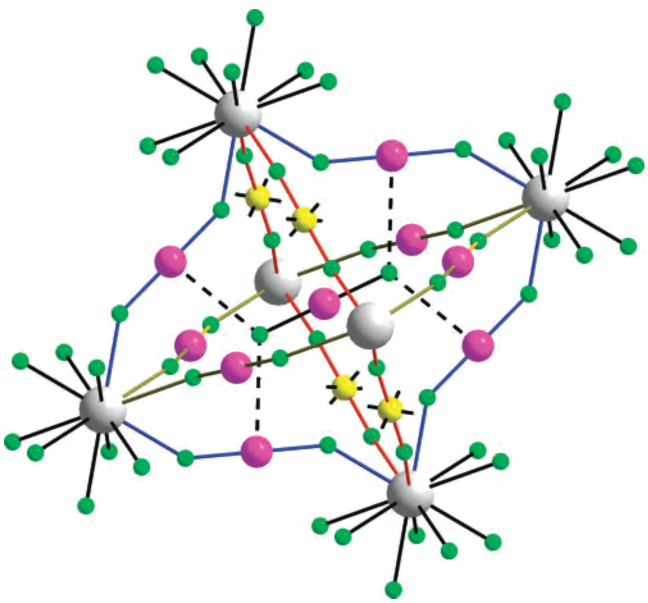

Figure 6. Uncoordinated XeF_2 molecule in the structure of $[Ba(XeF_2)_5][AsF_6]_2$.

(AsF_6 moiety) atoms. The 12 fluorine atoms form a nearly regular icosahedron about barium (Figure 5). The bridging nature of the AsF_6^- anions and the bridging XeF_2 molecules in $[Ba(XeF_2)_4][AsF_6]_2$ form a three-dimensional network, with the nonligating $Xe(1)F_2$ located in the cavities (Figure 6). The $Xe(1)F_2$ molecule, being nonligating to the barium atom, is fixed in the crystal space by four weak contacts (F1···Xe2 distance of 3.242(4) Å) to the bridging $Xe(2)F_2$ ligand (Figure 6). Similar to the SbF_6^- anion in $[Ba(XeF_2)_5][SbF_6]_2$,[21] the AsF_6^- anion in $[Ba(XeF_2)_5][AsF_6]_2$ exhibits tetragonal distortion with elongated $As-F_{bridge}$ bonds to the fluorine atoms that are trans-bridging barium centers. The crystal structure represents a static picture of the AsF_6^- anion in the crystal lattice, which is in contrast with the rapid reorientation of the anion on the NMR time scale.

Calculations. To assign ^{129}Xe and ^{19}F resonances to particular xenon and fluorine atoms in the crystal structure, shielding tensors of ^{129}Xe and ^{19}F were calculated for $[Mg(XeF_2)_4][AsF_6]_2$ at the BP86/TZ2P/ZSC level of theory (see Computational Details), using the unit cell of the single-crystal structure as a cluster model. We have also optimized the cluster at the BP86/TZ2P/ZSC level of theory for comparison. In addition, $^1J(^{129}Xe-^{19}F)$ coupling constants were calculated at the BP86/TZ2P/ZSC level of theory. The calculated and experimental isotropic chemical shifts, δ_{iso}, shielding anisotropies, $\Delta\sigma$, and asymmetries, η, for ^{19}F and ^{129}Xe are listed in Tables 2 and 3, respectively. The calculated and experimental $^1J(^{129}Xe-^{19}F)$ coupling constants are listed in Table 2.

The calculated $\delta_{iso}(^{19}F)$ values and $|^1J(^{129}Xe-^{19}F)|$ constants of the four bridging fluorine (F1−F4) environments are significantly lower and higher than those of the four terminal fluorines (F5−F8), respectively. This confirms that the fluorine environment of a terminal fluorine-on-xenon environment becomes more shielded and the $|^1J(^{129}Xe-^{19}F_{terminal})|$ constant increases upon coordination of XeF_2. The gap between the calculated ^{19}F chemical shifts for the bridging and terminal fluorines is 20 ppm, which contrasts the almost continuous experimental ^{19}F chemical shift distribution. This is likely a consequence of the extended structure of $[Mg(XeF_2)_4][AsF_6]_2$ and the influence of next neighbors on the shielding tensor that are not taken into account in the calculations. The ^{19}F shielding anisotropies are systematically overestimated by the calculations, while the asymmetry parameters for the terminal fluorines are underestimated. Again, these effects are likely to be caused by the neglect of interactions present in the extended structure. The negative sign of $^1J(^{129}Xe-^{19}F)$ for xenon(II) fluorides has previously been established by computational means and was reproduced for coordination compounds of XeF_2 in the present study.[15] The sizes of the $^1J(^{129}Xe-^{19}F)$ coupling constants are underestimated in these calculations.

The calculated $\delta_{iso}(^{129}Xe)$ values for the four xenon environments show that the chemical shift of one xenon environment, Xe2, is significantly lower than that of the other three xenon environments. This is in excellent agreement with the experimental finding of one xenon environment being distinctly different, while the other three could not be resolved from each other in the NMR spectrum (see Xenon-129 NMR Spectroscopy). The nearly axial symmetry of the ^{129}Xe shielding tensor is nicely reproduced by the computational results. However, the shielding anisotropies are overestimated in these calculations, as for $\Delta\sigma(^{19}F)$. The chemical shift tensor of ^{129}Xe is known to be extremely sensitive to changes in its environment, and nonbonded interactions in the crystal lattice are likely to have significant effects on the ^{129}Xe shielding tensor. Overall, the computations strongly support the assignment of the experimental NMR data.

Conclusion

Solid-state NMR spectroscopy was shown to be valuable in distinguishing between bridging and terminal coordination modes of coordinating XeF_2. Fluorine-19 is the preferred nucleus for such a study because the ^{19}F chemical shift is primarily dependent on the bridging or terminal nature while ^{129}Xe is dependent on nonbonded interactions in the solid state. In addition, the extremely large shielding anisotropy of ^{129}Xe renders ^{129}Xe NMR spectroscopy very insensitive and causes difficulties in measuring $^{1}J(^{129}\text{Xe}-^{19}\text{F})$ coupling constants. For all coordination compounds of known structure, each crystallographically different fluorine atom on Xe gave rise to a separate ^{19}F resonance. The AsF_6^- anions in four of the five coordination compounds were found to be rapidly reorienting on the NMR time scale, emulating perfectly octahedral environments, showing that the static picture of fixed AsF_6^- anions, suggested by X-ray crystallography, has to be revised. Chemical-shift calculations have provided assignments of ^{19}F and ^{129}Xe resonance to crystallographic fluorine and xenon sites.

Experimental Section

Sample Preparation and Handling. The $[Mg(XeF_2)_2][AsF_6]_2$, $[Mg(XeF_2)_4][AsF_6]_2$, and $[Ca(XeF_2)_{2.5}][AsF_6]_2$ adducts were synthesized as previously described.[3,4] A similar synthetic route as in the above cases was applied for preparation of $[Ba(XeF_2)_3][AsF_6]_2$ and $[Ba(XeF_2)_5][AsF_6]_2$. Both compounds were synthesized by the reaction between stoichiometric amounts of $Ba(AsF_6)_2$ and XeF_2 in anhydrous HF; molar ratios of $Ba(AsF_6)_2$ and XeF_2 were exactly 1:3 and 1:5, respectively. Anhydrous HF was pumped off on the vacuum system at − 30 °C. While cooling the solutions, some crystals formed in the reaction vessel, which, in the case of $[Ba(XeF_2)_5][AsF_6]_2$, could be used for single-crystal determination. Preparation details: 1.) $[Ba(XeF_2)_3][AsF_6]_2$: 0.814 g (1.6 mmol) of $Ba(AsF_6)_2$, 0.817 g (4.8 mmol) of XeF_2, 1.641 g (1.6 mmol) of product; 2.) $[Ba(XeF_2)_5][AsF_6]_2$: 0.591 g (1.15 mmol) of $Ba(AsF_6)_2$, 0.984 g (5.8 mmol) of XeF_2, 1.596 g (1.2 mmol) of product.

All samples prepared for NMR analysis were characterized as described in the literature. The $[Mg(XeF_2)_2][AsF_6]_2$ and $[Mg(XeF_2)_4][AsF_6]_2$ coordination compounds were checked by Raman spectroscopy and X-ray powder diffraction[3] while $[Ca(XeF_2)_{2.5}][AsF_6]_2$ was checked by Raman spectroscopy.[4] Raman spectra of the barium compounds were also recorded and are given in the Supporting Information (Figure S4). The Raman spectrum of $[Ba(XeF_2)_5][AsF_6]_2$ is very similar to the previously reported spectrum of $[Ba(XeF_2)_5][SbF_6]_2$[21] with the exception of the bands attributable to the anion.

Samples were handled in the dry-nitrogen atmosphere of a dry box having a maximum water content of 0.1 ppm of water vapor (Vacuum Atmospheres). Inserts were fabricated from FEP (a copolymer of perfluorinated polypropylene and polyethylene) as previously described[12] and placed inside a conventional 4 mm o.d. zirconia rotor.

NMR Spectroscopy. Solid-state NMR spectra were recorded on a Varian INOVA 500 (11.744 T) spectrometer equipped with a Sun workstation. The ^{19}F and ^{129}Xe NMR spectra were obtained using a Varian 4-mm HFXY MAS T3 probe tuned to 469.756 and 138.555 MHz, respectively. Spectra were acquired at variable spinning speeds between 12 and 16 kHz, in order to identify all isotropic signals, which were, then, used for spectral simulation. Free induction decays for the ^{129}Xe (^{19}F) spectra were accumulated with spectral-width settings of 1.6 MHz (400 kHz). The number of transients accumulated for the ^{129}Xe (^{19}F) spectra were between 40,000 and 180,000 (200 and 3,400) using pulse widths of 0.75 (3) μs. Fluorine-19 decoupled ^{129}Xe NMR spectra were recorded using the TPPM decoupling mode. The ^{19}F spectra were referenced to external neat $CFCl_3$, the ^{129}Xe spectra were referenced to neat $XeOF_4$ using an external sample of neat TMS and the absolute frequency of $XeOF_4$ (Ξ = 27.810184 MHz).[22]

Spectral Simulations. MAS NMR spectra were simulated using the *SIMPSON* program.[23] The ^{19}F NMR spectra were simulated as a superposition of the ^{129}Xe-coupled and uncoupled spin systems. Dipolar coupling constants (R_{DD}) of 4800 Hz (F−Xe) and 4000 Hz (F−As) were used in all simulations. The analysis of the experimental spectra did not allow for the determination of R_{eff}, which is different from R_{DD}, as a consequence of signal overlap with the fluoropolymer background. Varying ΔJ and thereby R_{eff} in the spectral simulations did not result in any apparent differences between the experimental and simulated spectra.

Single-Crystal Structure Determination. Single-crystal data were collected using a Mercury CCD area detector coupled to a Rigaku AFC7 diffractometer with graphite monochromated Mo Kα radiation at −73 °C. The data were corrected for Lorentz and polarization effects. A multiscan absorption correction was applied to data sets. Data were processed using the *CrystalClear* software suite.[24] The structure was solved using direct methods by the *SIR92* program[25] implemented in program package *TeXsan*[26] and expanded by Fourier techniques. Full-matrix least-squares refinement of F^2 was performed using the *SHELXL97* program.[27]

Computational Details. Most of the DFT calculations for shielding constants and spin−spin coupling constants were performed with the 2005 version of the *Amsterdam Density Functional* (ADF)[28−30] package. For comparison, we have also performed computations of ^{19}F chemical shift with the *Gaussian03* (G03)[31] program. The Becke 88[32] exchange plus the Perdew 86[33] correlation (BP) non-hybrid functional along with the Vosko-Wilk-Nusair[34] local density approximation were used for ADF calculations. The

(22) Schumacher, G. A.; Schrobilgen, G. J. *Inorg. Chem.* **1984**, *23*, 2923−2929.

(23) Bak, M.; Rasmussen, J. T.; Nielsen, N. C. *J. Magn. Res.* **2000**, *147*, 296−330.

(24) *CrystalClear*; Rigaku Corporation: The Woodlands, TX, 1999.

(25) *SIR92*: Altomare, A.; Cascarano, G.; Giacovazzo, C.; Guagliardi, A. *J. Appl. Crystallogr.* **1993**, *26*, 343−350.

(26) *TeXsan for Windows*, Single Crystal Structure Analysis Software, version 1.06; Molecular Structure Corporation: The Woodlands, TX, 1997−1999.

(27) Sheldrick, G. M. *SHELX97-2*, Program for Crystal Structure Analysis, release 97-2; University of Göttingen: Göttingen, Germany, 1998.

(28) Fonseca Guerra, C.; Visser, O.; Snijders, J. G.; te Velde, G.; Baerends, E. J. In *Methods and Techniques for Computational Chemistry*; Clementi, E., Corongiu, C., Eds.; STEF: Cagliari, Italy, 1995; pp 303−395.

(29) te Velde, G.; Bickelhaupt, F. M.; Baerends, E. J.; van Gisbergen, S. J. A.; Fonseca Guerra, C.; Snijders, J. G.; Ziegler, T. *J. Comput. Chem.* **2001**, *22*, 931−967.

(30) (a) Baerends, E. J. et al. *Amsterdam Density Functional*; Theoretical Chemistry, Vrije Universiteit: Amsterdam, 2005. http://www.scm.com. (b) Autschbach, J.; Ziegler, T. *J. Chem. Phys.* **2000**, *113*, 9410−9418. (c) Autschbach, J.; Ziegler, T. *J. Chem. Phys.* **2000**, *113*, 936−947. (d) Wolff, S. K.; Ziegler, T.; van Lenthe, E.; Baerends, E. J. *J. Chem. Phys.* **1999**, *110*, 7689−7698.

(31) Frisch, M. J.; Trucks, G. W.; Schlegel, H. B.; Scuseria, G. E.; Robb, M. A.; Cheeseman, J. R.; Montgomery, J. A., Jr.; Vreven, T.; Kudin, K. N.; Burant, J. C.; Millam, J. M.; Iyengar, S. S.; Tomasi, J.; Barone, V.; Mennucci, B.; Cossi, M.; Scalmani, G.; Rega, N.; Petersson, G. A.; Nakatsuji, H.; Hada, M.; Ehara, M.; Toyota, K.; Fukuda, R.; Hasegawa, J.; Ishida, M.; Nakajima, T.; Honda, Y.; Kitao, O.; Nakai, H.; Klene, M.; Li, X.; Knox, J. E.; Hratchian, H. P.; Cross, J. B.; Bakken, V.; Adamo, C.; Jaramillo, J.; Gomperts, R.; Stratmann, R. E.; Yazyev, O.; Austin, A. J.; Cammi, R.; Pomelli, C.; Ochterski, J. W.; Ayala, P. Y.; Morokuma, K.; Voth, G. A.; Salvador, P.; Dannenberg, J. J.; Zakrzewski, V. G.; Dapprich, S.; Daniels, A. D.; Strain, M. C.; Farkas, O.; Malick, D. K.; Rabuck, A. D.; Raghavachari, K.; Foresman, J. B.; Ortiz, J. V.; Cui, Q.; Baboul, A. G.; Clifford, S.; Cioslowski, J.; Stefanov, B. B.; Liu, G.; Liashenko, A.; Piskorz, P.; Komaromi, I.; Martin, R. L.; Fox, D. J.; Keith, T.; Al-Laham, M. A.; Peng, C. Y.; Nanayakkara, A.; Challacombe, M.; Gill, P. M. W.; Johnson, B.; Chen, W.; Wong, M. W.; Gonzalez, C.; Pople, J. A. *Gaussian 03*, revision B.05; Gaussian, Inc.: Pittsburgh, PA, 2003.

zeroth-order regular approximation (ZORA)[35,36] has been selected in the ADF computations to incorporate relativistic effects. The triple-ζ doubly polarized (TZ2P) Slater-type basis set from the ADF library has been applied in all ZORA calculations. Bagno and Saielli have previously reported that the ZORA/TZ2P combination yields satisfactory accuracy for calculated chemical shifts and spin−spin coupling constants of xenon and fluorine.[37] We have performed "scalar" ZORA (ZSC, i.e., without spin−orbit coupling) as well as ZORA spin−orbit (ZSO) computations to assess the importance of relativistic effects on the shielding constants. For *J* couplings, the ZSC level was deemed sufficient for the purpose of this study, and we have omitted the expensive calculation of the usually negligible spin−dipole term. The validity of this approximation for *J*-coupling calculations is supported by a large set of available benchmark data on compounds containing heavy elements.[38] For calculations of fluorine chemical shifts with the G03 code, the IGLO-III basis was employed for F, the DZVP basis for Xe, and the 6-311G* basis for other atoms.[39] In the G03 calculations, Becke's three-parameter hybrid functional (B3LYP)[40] was applied in these calculations to assess the importance of using a hybrid functional. For the sake of brevity, the results of the G03 calculations are not shown here. The comparison of relativistic (scalar vs spin−orbit ZORA) with nonrelativistic data and a comparison of hybrid DFT vs non-hybrid DFT has been made to confirm that (i) a meaningful assignment of the ^{19}F shifts can be made based on non-hybrid DFT computations for the systems under scrutiny and (ii) that spin−orbit relativistic effects on the fluorine chemical shifts are relatively small for the clusters that were computed. However, the inclusion of spin−orbit effects improved the agreement with experiment for the fluorine shifts. Overall, the results obtained at the ZSO level of theory agreed best with experiment. ^{19}F and ^{129}Xe chemical shifts were referenced to calculated shielding constants of $CFCl_3$ and $XeOF_4$, respectively.

(32) Becke, A. D. *Phys. Rev. A: At., Mol., Opt. Phys.* **1988**, *38*, 3098−3100.
(33) Perdew, J. P. *Phys. Rev. B: Condens. Matter Mater. Phys.* **1986**, *33*, 8822−8824.
(34) Vosko, S. H.; Wilk, L.; Nusair, M. *Can. J. Phys.* **1980**, *58*, 1200−1211.
(35) van Lenthe, E.; Baerends, E. J.; Snijders, J. G. *J. Chem. Phys.* **1993**, *99*, 4597−4610.
(36) Dyall, K.; van Lenthe, E. *J. Chem. Phys.* **1999**, *111*, 1366−1372.
(37) Bagno, A.; Saielli, G. *Chem.*−*Eur. J.* **2003**, *9*, 1486−1495.
(38) (a) Autschbach, J. In *Calculation of NMR and EPR Parameters. Theory and Applications*; Kaupp, M., Bühl, M., Malkin, V. G., Eds.; Wiley-VCH: Weinheim, Germany, 2004; pp 227−247. (b) Autschbach, J.; Ziegler, T. In *Calculation of NMR and EPR Parameters. Theory and Applications*; Kaupp, M., Bühl, M., Malkin, V. G., Eds.; Wiley-VCH: Weinheim, Germany, 2004; pp 249−264.
(39) Basis sets were obtained from the *Extensible Computational Chemistry Environment Basis Set Database*, version 02/02/06, as developed and distributed by the Molecular Science Computing Facility, Environmental and Molecular Sciences Laboratory, which is part of the Pacific Northwest Laboratory, P.O. Box 999, Richland, WA 99352, and funded by the U.S. Department of Energy. The Pacific Northwest Laboratory is a multiprogram laboratory operated by Battelle Memorial Institute for the U.S. Department of Energy under Contract DE-AC06-76RLO 1830. Contact Karen Schuchardt for further information.
(40) Becke, A. D. *J. Chem. Phys.* **1993**, *98*, 5648−5652.

Acknowledgment. We thank the Natural Sciences and Engineering Research Council of Canada (M.G. and P.H.), the University of Lethbridge (M.G. and P.H.), the Slovenian Research Agency (M.T., E.G., and B.Ž.), AD Futura (E.G.), and the Alberta Network for Proteomics Innovation (M.G. and P.H.) for support of this work. We also thank Drs. Albert Cross and Dinu Iuga for their help in the acquisition of the solid-state NMR spectra. J.A. acknowledges support from the Center of Computational Research at SUNY Buffalo and is grateful for financial support from the CAREER program of the National Science Foundation (Grant No. CHE-0447321).

Supporting Information Available: Figures of the ^{19}F MAS NMR spectra of $[Ca(XeF_2)_{2.5}][AsF_6]_2$ (Figure S1), $[Ba(XeF_2)_3][AsF_6]_2$ (Figure S2), and $[Ba(XeF_2)_5][AsF_6]_2$ (Figure S3) and Raman spectra of $[Ba(XeF_2)_5][AsF_6]_2$ and $[Ba(XeF_2)_3][AsF_6]_2$ (Figure S4); X-ray crystallographic files, in CIF format, for the structure of $[Ba(XeF_2)_5][AsF_6]_2$ and for the resolved structure of $[Ba(XeF_2)_5][SbF_6]_2$ in the space group *Fmmm*. This material is available free of charge via the Internet at http://pubs.acs.org.

IC700557M